Two-body fragmentation dynamics of N_2O^{q+} ($q = 2, 3$) induced by electron-capture collisions with 5.7-keV/u Xe^{15+}

Lei Chen,[1] Xu Shan,[1,*] Xi Zhao,[1] Xiaolong Zhu,[2] Xiaoqing Hu,[3] Yong Wu,[3,†] Wentian Feng,[2] Dalong Guo,[2]
Ruitian Zhang,[2] Yong Gao,[2] Zhongkui Huang,[2] Jianguo Wang,[3] Xinwen Ma,[2,‡] and Xiangjun Chen[1]

[1]*Hefei National Laboratory for Physical Sciences at the Microscale and Department of Modern Physics,*
University of Science and Technology of China, Hefei 230026, China
[2]*Institute of Modern Physics, Chinese Academy of Sciences, Lanzhou 730000, China*
[3]*Institute of Applied Physics and Computational Mathematics, Chinese Academy of Engineering Physics, Beijing 100094, China*

Two-body fragmentation of N_2O^{q+} ($q = 2, 3$) induced by electron-capture collision of 5.7-keV/u Xe^{15+} is studied. Through the triply coincident measurement on ion-pair fragments with the scattered projectile and the correlation analysis on the ion-pair time of flight and momentum conservation, we have clearly identified 12 reaction channels for the formation and dissociation of N_2O^{2+} and N_2O^{3+}. The fraction ratios for these channels and the corresponding kinetic energy release (KER) distributions for the ion-pair products have been obtained. Calculations of the potential energy curves of N_2O^{3+} for the N-N and N-O bond stretches are performed using the complete active space self-consistent field method. The KER spectra for the two-body fragmentation of $N_2O^{2+} \rightarrow N^+ + NO^+$ and $N_2^+ + O^+$ can be explained by the decay via the $X\ ^3\Sigma^-$ and $1\ ^3\Pi$ states, and the major peaks or structures observed in the KER spectra for $N_2O^{3+} \rightarrow N^+ + NO^{2+}$ can be attributed to the $1\ ^2\Pi$, $2\ ^2\Pi$, and $2\ ^2\Sigma^-$ states, whereas those in the KER spectra for $N_2O^{3+} \rightarrow O^+ + N_2^{2+}$ are mainly contributed from the $1\ ^2\Pi$, $3\ ^2\Pi$, and $4\ ^2\Pi$ states. In addition, we found that the KER structures for the same ion-pair products are not sensitive to the number of electrons stabilized at the projectile, but the KER intensities are clearly dependent on it. The mechanism of multielectron captures of the projectile to form the transient multicharged molecular ions and the following projectile stabilization with or without autoionizing cascades is proposed to explain it.

I. INTRODUCTION

Electron transfer and emission, as well as the following dissociation processes of molecules induced by the highly charged ion (HCI) collision are of importance both in fundamental research and in their applications, particularly to molecular physics [1] and biological studies on radiation damage [2]. Over the past decades, reaction microscope or coincidence momentum imaging techniques [3,4] have been demonstrated to be feasible to reconstruct the three-dimensional momentum vectors for charged particles formed in collision processes. As a result, numerous HCI experiments have been performed on molecular systems from simple diatomic molecules like N_2 [5–10] and CO [11–14] to triatomic molecules such as CO_2 [1,15–18], OCS [19,20], CS_2 [16,21], H_2O [22,23], and even several polyatomic molecules [7,24–26]. Most of these studies focused on identifying the dissociation channels and reconstructing the structure of precursor molecular ions with the aid of the measured time of flight (TOF) and the kinetic energy release (KER) of the fragments, but only a few works paid attention to the electron transfer in ion-molecule collisions and its influence on the following fragmentation of molecular ions [7–13,18].

In slow collisions of He^{2+} and Ar^{3+} with N_2, Ehrich *et al.* [7] found that the KER distributions of two fragment N^+ ions strongly depend on the number of electrons captured by the projectile ions, i.e., with increasing number of captured electrons, the position of maximum is shifted towards lower energies and the width of KER distributions becomes smaller and smaller. Whereas in the case of high-energy collisions of 97-MeV Ar^{14+} and CO [27], the average value of KER obtained in one-electron-capture collision was found to be considerably larger than that in the pure ionization process in which the projectile charge state does not change. A similar remark is also reported in charge-changing ion-molecule collisions of 2-MeV C^+ and N_2 [10], where the KER was found to differ significantly in electron loss and capture processes of the projectile. These studies implied that the fragmentation dynamics of molecular ions could be strongly dependent on the particular collision processes and parameters including the projectile charge, velocity, and type. Thus, further investigations on this issue, especially extending to polyatomic molecules, are highly desirable.

Nitrous oxide (N_2O), a well-known greenhouse gas, is one of the dominant ozone-depleting substances emitted through human activities [28]. In addition, the N_2O molecule has a linear asymmetrical triatomic structure where two N atoms are not equivalent in the chemical site. All these make it interesting to study the dissociative ionization of N_2O. Fragmentation of N_2O^{q+} induced by the interactions with electrons [29–32], photons [32–37], and intense laser fields [38–40] has been

*xshan@ustc.edu.cn
†wu_yong@iapcm.ac.cn
‡x.ma@impcas.ac.cn

studied extensively. Theoretical studies for the potential energy surfaces of multicharged molecular ions are restricted to N_2O^{2+} [34,35,41]. On the other hand, less attention was paid to the ion-induced fragmentation of N_2O. The investigations available on two-body dissociation of N_2O were conducted by Siegmann *et al.* [42] in fast collision with 5.9-MeV/u Xe^{43+} and Wang *et al.* [43] in collisions of 15–30-keV H^-, C^-, and O^-. The complete three-body Coulomb fragmentation of N_2O^{q+} ($q = 3, 4, 5$) is studied by Werner *et al.* [44] in collisions with 3.6-MeV/u Au^{50+}, 5.9-MeV/u Xe^{18+}, and 5.9-MeV/u Xe^{43+}. Very recently, Khan *et al.* [45] also reported their study on the three-body fragmentation of N_2O^{q+} ($3 \leqslant q \leqslant 7$) in collisions with 1 atomic unit (a.u.) Ar^{8+} (1 MeV) and Xe^{15+} (3.2 MeV). However, in these works, the effects of electron capture in ion-N_2O collision on the fragmentation of molecular ions have not been studied so far. In addition, the accurately measured KER and calculated potential energy surfaces, particularly for N_2O^{3+}, are expected to reveal the specific decay pathway and dynamics.

We report here a detailed study on two-body fragmentation of N_2O^{q+} ($q = 2, 3$) induced by electron-capture (EC) collisions of 5.7-keV/u Xe^{15+}. The momenta of fragment ions are measured in coincidence with the charge-changed projectile by a reaction microscope setup. Through the correlation analysis on the TOF and momentum conservation of ion-pair fragments, 12 reaction channels for the EC-induced ion-pair dissociations are identified and the corresponding KER distributions are derived. Calculations of the potential energy curves of N_2O^{3+} for N-N and N-O bond stretches are performed using the complete active space self-consistent field (CASSCF) method. We explored the two-body fragmentation mechanism of N_2O^{2+} and N_2O^{3+} in view of the measured KER spectra and the calculations. Furthermore, the effect of electron capture on the fragmentation of molecular ions is also analyzed.

II. EXPERIMENTAL METHODS

The measurements were carried out using a reaction microscope mounted on the 320-kV platform for multidisciplinary research with highly charged ions at the Institute of Modern Physics, Chinese Academy of Science, Lanzhou. The details of the experimental setup have been presented elsewhere [46,47]. Briefly, Xe^{15+} ions were extracted from a 14.5-GHz electron cyclotron resonance ion source and accelerated to 750 keV. After being collimated by two sets of adjustable slits and purified by several sets of electrostatic deflectors, the ion beam was transported to the target chamber and intersected with a cold supersonic N_2O gas jet. The diameter of the molecular beam at the interaction zone is about 2 mm, and the estimated target density is approximately 10^{11} particles/cm^3 with a driving pressure of 6 bars. The recoil ions (i.e., molecular fragments) formed in the collisions were extracted and accelerated toward the time- and position-sensitive detector (PSD-R) by a Wiley McLaren-type TOF spectrometer [48]. The projectile ions were charged-state analyzed by a magnetic deflector downstream of the interaction zone. The primary projectile ions were collected by a Faraday cup, whereas the charge-changed ions were detected by another position-sensitive detector (PSD-P). The signal from PSD-P

triggered the data acquisition system, and the recoil ions were recorded in coincidence with the scattered projectile ions. Thus, pure target ionization reactions were eliminated in the present experiment. All time- and position-sensitive detectors mentioned above consisted of a pair of microchannel plates and a delay line anode. The multihit response of such detectors allows one to reconstruct the momentum vector of each fragment ion from the time of flight and the detection position. Through the correlation analysis on the TOF and momentum conservation of ion-pair fragments, as well as the charge states of the scattered projectile, the reaction channels for the EC-induced two-body Coulomb explosion can be determined.

III. COMPUTATIONAL METHODS

Since the potential energy curves (PECs) of N_2O^{2+} have been studied before [34,35] by using the internally contracted multireference configuration interaction (MRCI) method and those of N_2O^{3+} are not available in the literature. In this work, the calculations of PECs for collinear geometries of N_2O^{3+} along with N-N and N-O bond stretches are performed using the CASSCF method [49,50], a combination of an SCF computation with a full configuration interaction involving a subset of the orbitals (known as the active space), in which all the states included in the concerned configuration active space are optimized simultaneously and both wave functions and energies are converged to second order. Here the active space is comprised of all valence orbitals, totally about 85 000 configuration state functions are considered in the PECs calculations for two $^2\Sigma^+$ states, three $^2\Sigma^-$ states, two $^2\Delta$ states, and five $^2\Pi$ states. In addition, the orbital wave functions are expanded on Dunning's cc-pV5Z (i.e.,$15s7p1d$ contracted to $4s3p1d$) basis set [51], which describes the core-valence correlation and polarization effect well. The present PECs calculations are carried out using the MOLPRO 2010 software package [52].

IV. RESULTS AND DISCUSSION

A. Ion-ion coincidence maps and identification of reaction channels

Figure 1(a) shows a two-dimensional coincidence map between the TOF of molecular fragments and the position of charge-changed projectile ions obtained from the 5.7-keV/u Xe^{15+} and N_2O collision experiment. In Fig. 1(a), two charge states of the final projectile ion could be clearly identified, namely, Xe^{14+} and Xe^{13+}. The total TOF spectrum of fragment ions is illustrated in Fig. 1(b). One can see that various fragment ions from the dissociative ionization of N_2O can be resolved clearly. Figures 1(c) and 1(d) show the two-dimensional TOF coincidence maps of ion-pair fragments for Xe^{14+} and Xe^{13+} scattered projectiles, from which a series of reaction channels can be resolved independently. In the present work, we concentrate on the two-body complete Coulomb explosion channels and study the EC selective dissociation dynamics of N_2O^{2+} and N_2O^{3+}. With the help of ion-pair TOF correlation maps in Figs. 1(c) and 1(d), 12 channels for the EC-induced N_2O^{2+} and N_2O^{3+} fragmentation are identified and presented below. In these reaction channels, the scattered projectile finally held one or two electrons, and the electron emission process is also accompanied except for the Ch(3) and Ch(4) channels. Here,
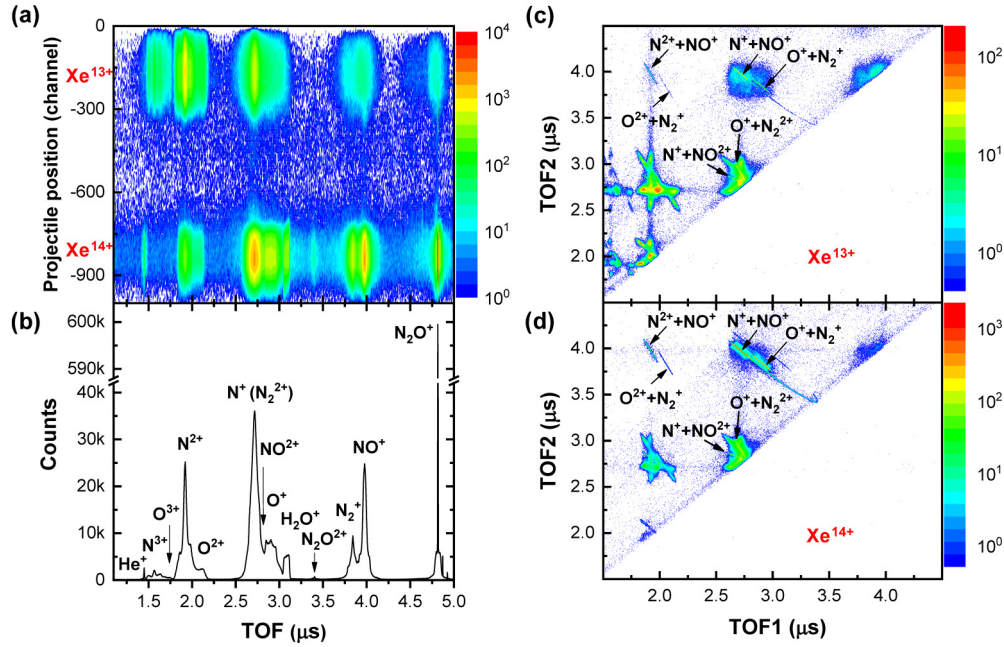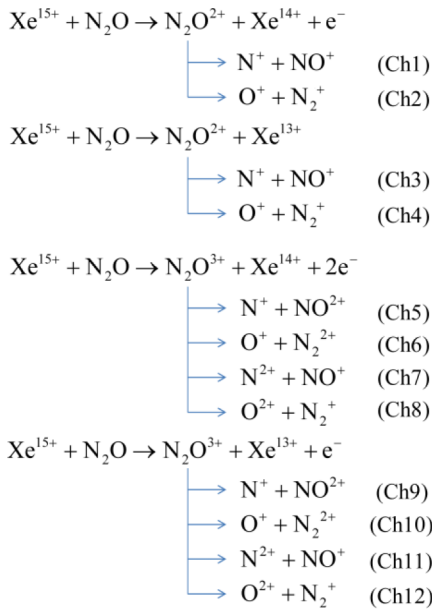
FIG. 1. (a) Two-dimensional coincidence map between the time of flight of fragment ions and the position of the projectile ion after capturing electrons; (b) one-dimensional time of flight spectrum for the first hit ions, (c), (d) ion-ion coincidence maps between the first hit ions and the second ones.

we denote the processes producing Xe^{14+} and Xe^{13+} as the single- and double-electron capture (SC and DC) collisions of the Xe^{15+} projectile, respectively.

$$\text{Xe}^{15+} + \text{N}_2\text{O} \rightarrow \text{N}_2\text{O}^{2+} + \text{Xe}^{14+} + e^-$$

$$\longmapsto \text{N}^+ + \text{NO}^+ \quad \text{(Ch1)}$$
$$\longmapsto \text{O}^+ + \text{N}_2^+ \quad \text{(Ch2)}$$

$$\text{Xe}^{15+} + \text{N}_2\text{O} \rightarrow \text{N}_2\text{O}^{2+} + \text{Xe}^{13+}$$

$$\longmapsto \text{N}^+ + \text{NO}^+ \quad \text{(Ch3)}$$
$$\longmapsto \text{O}^+ + \text{N}_2^+ \quad \text{(Ch4)}$$

$$\text{Xe}^{15+} + \text{N}_2\text{O} \rightarrow \text{N}_2\text{O}^{3+} + \text{Xe}^{14+} + 2e^-$$

$$\longmapsto \text{N}^+ + \text{NO}^{2+} \quad \text{(Ch5)}$$
$$\longmapsto \text{O}^+ + \text{N}_2^{2+} \quad \text{(Ch6)}$$
$$\longmapsto \text{N}^{2+} + \text{NO}^+ \quad \text{(Ch7)}$$
$$\longmapsto \text{O}^{2+} + \text{N}_2^+ \quad \text{(Ch8)}$$

$$\text{Xe}^{15+} + \text{N}_2\text{O} \rightarrow \text{N}_2\text{O}^{3+} + \text{Xe}^{13+} + e^-$$

$$\longmapsto \text{N}^+ + \text{NO}^{2+} \quad \text{(Ch9)}$$
$$\longmapsto \text{O}^+ + \text{N}_2^{2+} \quad \text{(Ch10)}$$
$$\longmapsto \text{N}^{2+} + \text{NO}^+ \quad \text{(Ch11)}$$
$$\longmapsto \text{O}^{2+} + \text{N}_2^+ \quad \text{(Ch12)}$$

The relative fractions of the 12 reaction channels identified by the present experiment are also determined by using the

corrected counts after the ion-pair momentum correlation and conservation, which are listed in Table I. One can see that the SC-induced dissociative reactions for both N$_2$O^{2+} and N$_2$O^{3+} are dominant. In addition, for two dissociative channels of N$_2$O^{2+}, the ratios of the SC and DC reactions are almost the same as 97:3, while for four dissociative channels of N$_2$O^{3+}, the ratios between the SC and DC are approximately equal to 85:15, a little lower than for the case of N$_2$O^{2+}.

It is noted that the ratio of N$_2$O^{2+} breakup to N$^+$ + NO$^+$ and O$^+$ + N$_2^+$ has been studied extensively by electron, ion, and photon collision experiments [30,33,34,40,42], as well as the simulation [41]. One can see from Table II that the present ratio of about 65:35 is very close to the previous data of 59:41 from the ion experiment [42], but smaller than those from electron (75:25) [30] and photon experiments (80:20) [33,34]. The discrepancy could be qualitatively understood in view of the different reaction mechanism to form N$_2$O^{2+} excited-state populations among the various experiments, i.e., electron-capture processes in ion-molecule collision and pure ionizations in electron or photon collisions.

B. Dissociation of N$_2$O^{2+}

As presented above, two kinds of ion-pair dissociation channels of N$_2$O^{2+} have been identified, i.e., N$_2$O^{2+} → N$^+$ + NO$^+$ and N$_2$O^{2+} → O$^+$ + N$_2^+$, corresponding to four

TABLE I. Relative ion-pair fractions for 12 reaction channels observed in 5.7-keV/u Xe^{15+}-N$_2$O collision.

Reaction	N$_2$O^{2+}		N$_2$O^{3+}			
	N$^+$ + NO$^+$	O$^+$ + N$_2^+$	N$^+$ + NO^{2+}	O$^+$ + N$_2^{2+}$	N^{2+} + NO$^+$	O^{2+} + N$_2^+$
SC	56.05%	30.45%	3.41%	3.77%	2.06%	0.13%
DC	1.73%	0.82%	0.55%	0.63%	0.38%	0.02%

TABLE II. Relative abundances for $N^+ + NO^+$ and $O^+ + N_2^+$ of N_2O^{2+} fragmentation determined by various experiments.

Channel	Present		5.9-MeV/u Xe^{43+} ions [42]	10-keV electron [30]	40-eV photon [33]	24–100 nm photon [34]	800-nm intense laser [40]	Theoretical prediction [41]
	SC	DC						
$N^+ + NO^+$	65%	68%	59%	74%	80%	79%	75.5%	75%
$O^+ + N_2^+$	35%	32%	41%	26%	20%	21%	24.5%	25%

reaction channels (Ch1–Ch4). The specific KER distributions for these channels are shown in Fig. 2, respectively, and the noticeable peaks or shoulders are observed clearly. In addition, for the same ion-pair fragments induced by the SC and DC processes, the shapes of the KER distributions, particularly at the positions of peaks and shoulders, are almost the same, indicating that the KER distributions of N_2O^{2+} fragmentation are not sensitive to different reaction processes in the present 5.7-keV/u Xe^{15+} collisions. This behavior is quite different from the previous observations of Ehrich *et al.* [7] in slow collisions of 300-keV Ar^{3+} with N_2 and those of Watson *et al.* [27] in fast collisions of 97-MeV Ar^{14+} with CO, in which they found the clear dependence of the KER distributions on the number of electrons captured by the projectile, but contrary behaviors were revealed by these two experiments. We conjecture that the present highly charged Xe^{15+} slow collision could allow the almost identical state populations of N_2O^{2+}, and therefore result in very similar behavior of KER distributions for the same ion-pair fragments.

In order to assign the structures observed in the KER spectra and reveal the specific pathway of N_2O^{2+} dissociations, the KER spectra for these channels are fitted by Gaussian functions using the least-squares method as shown in Fig. 2.

The positions of the major peaks and shoulders are determined and listed in Table III. As a comparison, KER values available in the literature [29–32,34,36,38–40,42] are also shown in Table III.

For $N_2O^{2+} \rightarrow N^+ + NO^+$, as shown in Fig. 2(a), the observed major peak at 6.8 eV is in good agreement with the previous measurements [29,38,40,42]. A broad peak or shoulder is also observed around 9.0 eV, but only Bhatt *et al.* [30] presented an indication at about 5.3 eV in their 10-keV electron collision experiment, where much lower KER values for the observed channels were reported than those in other works. According to the previous MRCI potential energy curves of N_2O^{2+} [35], the presently measured peak at 6.8 eV should be ascribed to the significant contribution of N_2O^{2+} ($1\ ^3\Sigma^-$) dissociating to $N^+(^3P) + NO^+(^1\Sigma^+)$ with respect to the lowest adiabatic threshold energy (28.79 eV) for this channel [53]. It is worth noting that the contribution to this peak from the $1\ ^3\Pi$ state of N_2O^{2+} is also probable because it may decay along the N-N stretching direction via fluorescent transitions to the $1\ ^3\Sigma^-$ state and then dissociates [35,38]. The shoulder around 9.0 eV could be assigned to the contributions of N_2O^{2+} ($1\ ^1\Pi$, $1\ ^1\Sigma^-$) dissociating to $N^+(^1D) + NO^+(^1\Sigma^+)$ in view of the possible curve crossing
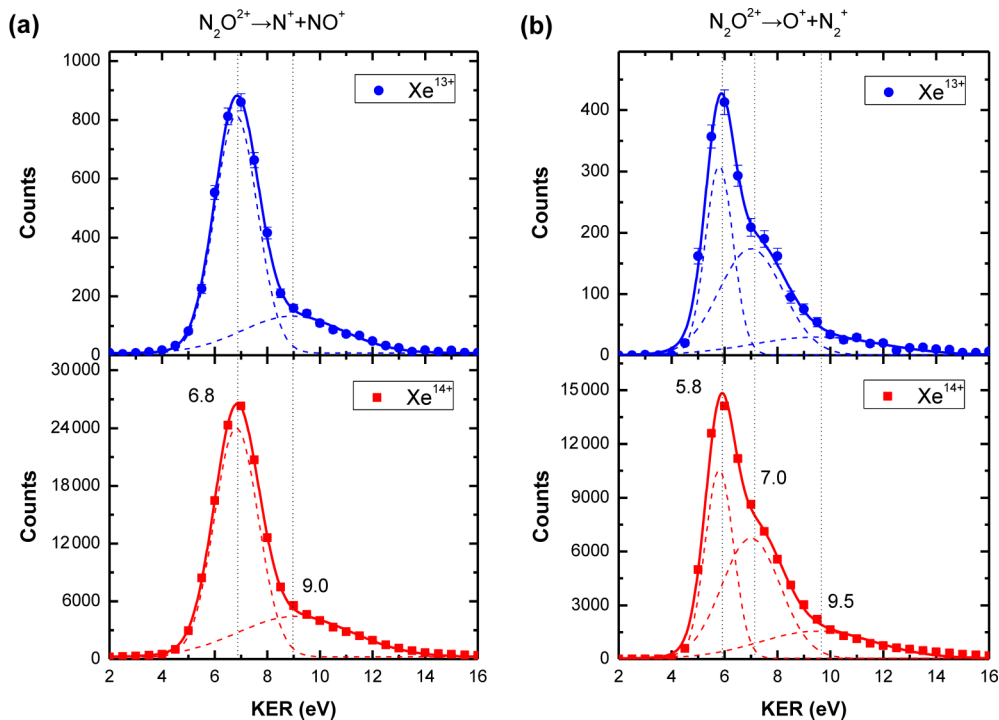

FIG. 2. The KER spectra for two-body dissociation of N_2O^{2+}: (a) $N^+ + NO^+$, (b) $O^+ + N_2^+$. Two Gaussian peaks in (a) and three in (b) (dashed lines) are used to fit the experimental data (circular and square solid dots) and the solid lines represent the sum of their fitting.

TABLE III. Comparison of KER peak values for various dissociation channels of N_2O^{2+} and N_2O^{3+} obtained by the present and previous experiments.

	KER (eV)												
	Ion impacts			Electron impacts				Ultraviolet light			Intense laser		
	Present		Ref. [42]	Ref. [31]	Ref. [32]	Ref. [29]	Ref. [30]	Ref. [32]	Ref. [36]	Ref. [34]	Ref. [38]	Ref. [39]	Ref. [40]
Channel	SC	DC											
$N^+ + NO^+$	6.8	6.8	7.0	6.3 ±1.0	7.2 ± 0.7	6.6 ± 0.2	4.0 ± 0.5	7.2 ± 0.4	6.4 ± 0.3	6.3 ± 0.3	6.8	6.5 ± 0.2	6.8 ± 0.2
	9.0	9.0					5.3 ± 0.6						
$O^+ + N_2^+$	5.8	5.8	5.0	3.2 ± 1.0	7.5 ± 1.5	5.9 ± 0.2	3.5 ± 0.4	7.4 ± 1.0	5.6 ± 0.5	3.2	5.8	5.6	6.2 ± 0.1
	7.0	7.0	6.5	5.8 ± 1.0		7.0 ± 0.2	4.4 ± 0.5			5.8	7.2		
	9.5	9.5		9.0 ± 1.0			5.6 ± 0.7			8.5			
$N^+ + NO^{2+}$	13.0	13.0				13.0 ± 0.2						11.3 ± 1.3	
	16.5	16.5											
	21.5	21.5											
$O^+ + N_2^{2+}$	12.0	12.0											
	15.0	15.0											
	17.0	17.0											
$N^{2+} + NO^+$	13.0	13.0			17.5 ± 3	13.2 ± 0.2	8.4 ± 1.0					11.9 ± 0.2	
	17.0	17.0											
	22.0	22.0											
$O^{2+} + N_2^+$	16.0	16.0				15.0 ± 2.0						12	
	23.0	23.0				22.0 ± 2.0							

of the $1\,^1\Pi$ and $1\,^1\Sigma^-$ states of N_2O^{2+}. However, a theoretically expected KER peak (12.7 eV) for this dissociation channel predicted by the pure Coulomb explosion (CE) model using localized point charges at equilibrium bond length is not observed in the present measurement, which agrees with the previous reports.

For the dissociation channel $N_2O^{2+} \rightarrow O^+ + N_2^+$, to model the KER spectra correctly, we fit each of them using three Gaussian-type peaks. Both KER spectra for the SC and DC collisions show a noticeable peak at 5.8 eV, a pronounced shoulder around 7.0 eV, and a high-energy tail above 9.5 eV, respectively. Our present observations on KER structures are in good accordance with the previous measurements by 5-keV electron impact (5.9, 7.0 eV) [29] and 750-nm intense laser experiments (5.8, 7.2 eV) [38], whereas Siegmann *et al.* [42], in the 5.9-MeV/u Xe⁴³⁺ collision experiment, observed two structures in the KER spectrum for this channel at 5.0 and 6.5 eV. Similar to the case of $N_2O^{2+} \rightarrow N^+ + NO^+$, all the measured KER values are lower than the value (12.2 eV) predicted by the CE model for this channel. In light of the MRCI calculations [35], the presently observed peak at 5.8 eV can be explained by the N_2O^{2+} ($X\,^3\Sigma^-$) decay into $O^+(^4S) + N_2^+(^2\Sigma_g^+)$ whose energy limit is 30.9 eV, while the shoulder around 7.0 eV should be attributed to the decay of the $N_2O^{2+}(1\,^3\Pi) \rightarrow O^+(^4S) + N_2^+(^2\Pi_u)$ pathway with the decay limit of 32.4 eV. A high-energy tail above 9.5 eV may be the contributions of other highly excited states of N_2O^{2+}, referred to as the mixture of states in the literature [35].

C. Dissociation of N_2O^{3+}

As described above, eight reaction channels for the SC- and DC-induced N_2O^{3+} dissociations (Ch5-Ch12) have been identified by using the TOF correlation and momentum conversation of ion-pair fragments. The momentum of center of

mass of the precursor ion is also used to eliminate the random coincidences from these complete CE channels. Figures 3(a)–3(d) show the KER distributions for these eight dissociation channels of N_2O^{3+}.

For the sake of studying the KER structures carefully, we used Gaussian-type peaks to fit the KER spectra for the eight channels. As shown in Fig. 3(a), for the $N_2O^{3+} \rightarrow N^+ + NO^{2+}$ pathway a sharp peak can be assigned to be 13.0 eV in both reaction processes, well agreeing with the value of Khan and Misra [29]. A broad peak around 16.5 eV is also clearly identified from the KER spectra, which was not observed in the previous experiments. The high-energy KER tail appearing around 21.5 eV is lower than the expected KER value (25.5 eV) predicted by the pure CE model. As for $N_2O^{3+} \rightarrow O^+ + N_2^{2+}$, a distinct peak at 15.0 eV and two shoulders around 12.0 and 17.0 eV are clearly recognized in the KER spectra for the SC and DC collisions. The CE model predicts a KER value of 24.4 eV for this channel, still much higher than the present measured values. As mentioned above, the present CE model is a simple model, only using localized point charges at the equilibrium bond length of N_2O, in which the simple repulsive potential may not well describe the PECs of molecular ions. Furthermore, for the formation of N_2O^{2+} or N_2O^{3+}, the outer-valence orbital electrons are not completely stripped. The delocalization of the remaining electrons will make the charge on each nucleus center deviate from integer values. Such factors may result in the discrepancy of KER values between the CE prediction and the measurement [54].

The KER distributions for the $N_2O^{3+} \rightarrow N^{2+} + NO^+$ are shown in Fig. 3(c), in which a major peak at 13.0 eV and a second peak at 17.0 eV are distinctly observed. Additionally, a higher KER tail around 22.0 eV seems visible. As can be seen in Table III, Hishikawa *et al.* [39] reported a peak around 11.9 ± 2.0 eV and Eland and Murphy [32] reported a peak around 17.5 ± 3.0 eV, whereas Khan *et al.* [29] reported a
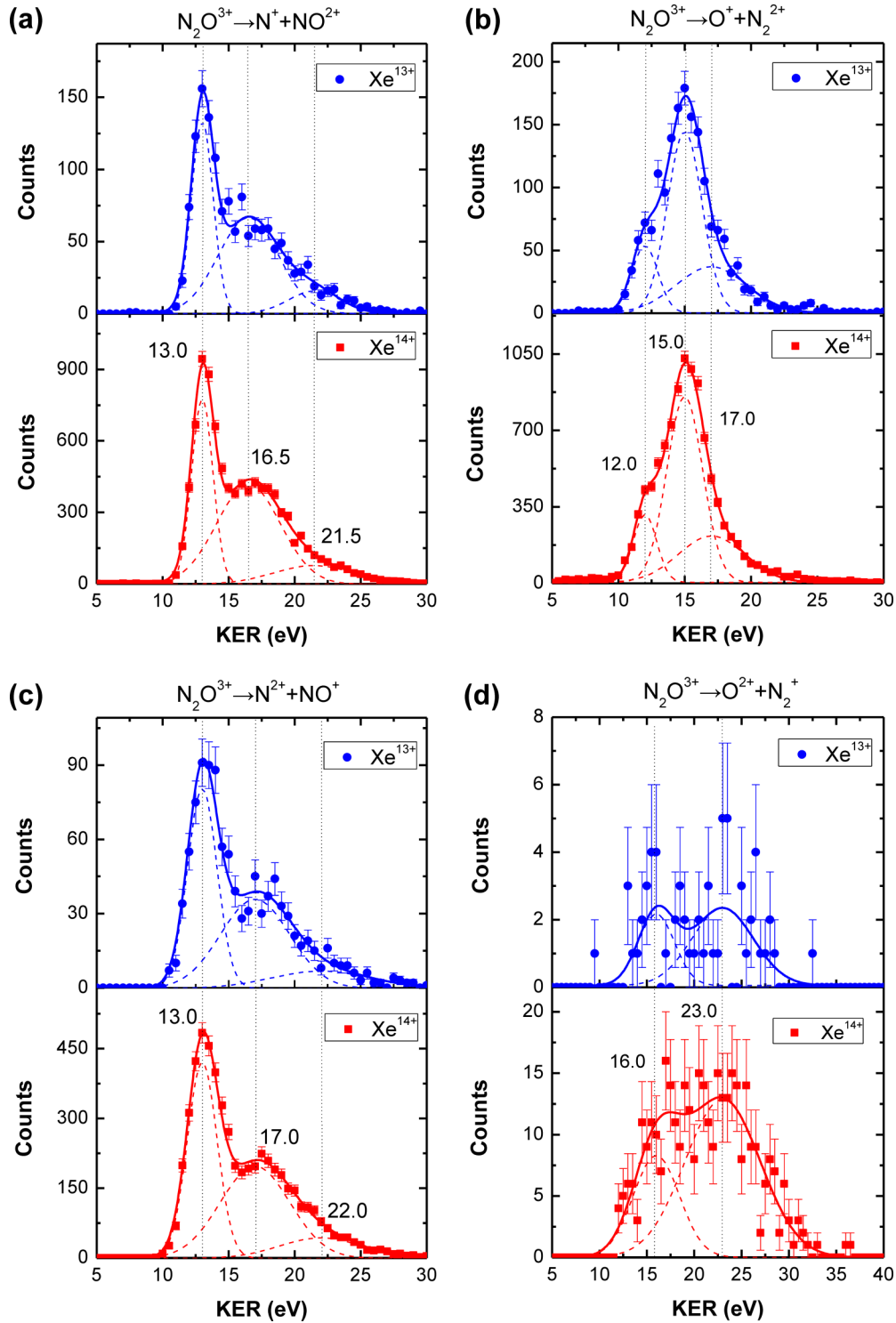
FIG. 3. The KER spectra for two-body dissociation of N_2O^{3+}: (a) $N^+ + NO^{2+}$, (b) $O^+ + N_2^{2+}$, (c) $N^{2+} + NO^+$, and (d) $O^{2+} + N_2^+$. Three Gaussian peaks in (a)–(c) and two in (d) (dashed lines) are used to fit the experimental data (circular and square solid dots) and the solid lines represent the sum of their fitting.

major peak around 11.8 eV. All these experimental values are lower than the prediction of the CE model (25.5 eV). It is noted that the characteristics of KER distributions for this decay pathway, which include three peaks and their positions, are very similar to those of $N_2O^{3+} \to N^+ + NO^{2+}$.

In Fig. 3(d), we present the KER distributions for the SC- and DC-induced $N_2O^{3+} \to O^{2+} + NO^+$ channels which can be identified clearly from the ion-ion coincidence map in Fig. 1. Due to the very small reaction probability relative to other N_2O^{3+} decay channels, the measured counts are quite
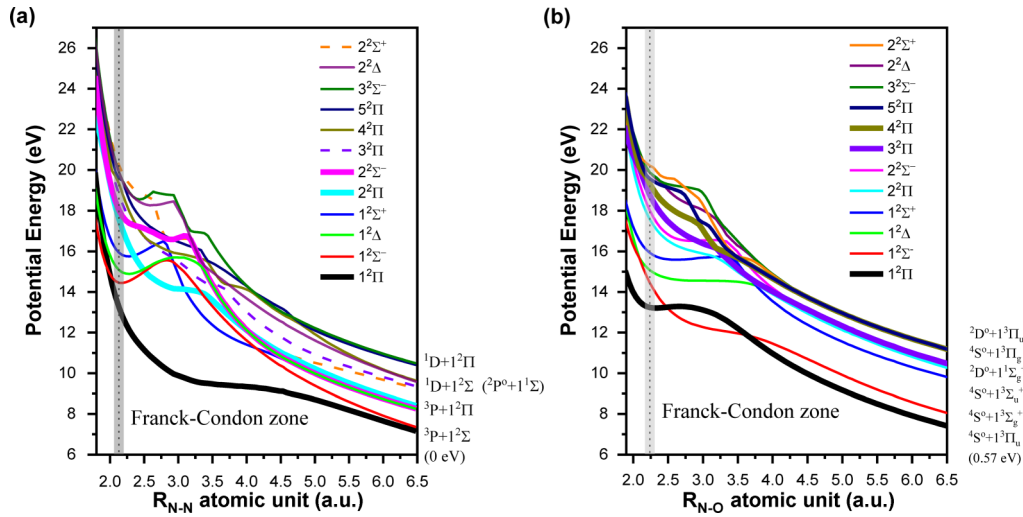
FIG. 4. Potential energy curves of N$_2$O^{3+} for (a) N-N and (b) N-O bond stretches. Vertical dashed lines and the shadow area represent the equilibrium bond lengths and the Franck-Condon zone of N$_2$O (X $^1\Sigma^+$), where vertical transitions may occur in view of the fast collision time (less than 10^{-16} s). Dissociation limits are shown on the right side of each panel.

low for this decay of N$_2$O^{3+}. However, two structures can be identified in both KER spectra at about 16.0 and 23.1 eV, close to the values of Khan *et al.* [29].

It is well known that the kinetic energy released by the fragmentation is directly linked with the electronic states of precursor molecular ions. In order to reveal the origin of KER peaks and understand the decay dynamics of N$_2$O^{3+}, we have calculated the potential energy curves for collinear geometries of N$_2$O^{3+} along N-N and N-O bond stretches at the CASSCF level of theory, where the N-O or N-N bond length is fixed at the equilibrium values of N$_2$O (X $^1\Sigma^+$), i.e., $R_{\text{N-N}} = 2.132$ a.u. and $R_{\text{N-O}} = 2.223$ a.u., respectively. Because of the complexity of N$_2$O^{3+} electronic states, it is very difficult to scan the potential surfaces for too many electronic states. In this work, only the electronic states with doublet multiplicity are taken into account. The calculated results are depicted in Fig. 4, and the dissociation limits are also included in each figure with the energy zero

point set at the lowest dissociation limit ($^3P + 1$ $^2\Sigma$). In Fig. 4(a), the potential wells for the 1 $^2\Sigma^-$, 1 $^2\Sigma^+$, and 1 $^2\Delta$ states of N$_2$O^{3+} along the N-N stretches can be seen, while these states of N$_2$O^{3+} along the N-O coordinates, as shown in Fig. 4(b), have no obvious potential wells. In addition, other states of N$_2$O^{3+} have no obvious potential barriers, indicating the repulsive or predissociative features. Table IV lists the low-lying electronic states of N$_2$O^{3+} and the corresponding KER values calculated according to their dissociation limits.

According to the present calculations in Table IV, the two peaks at 13.0 and 16.5 eV observed in Fig. 3(a) in experimental KER spectra for the N$_2$O$^{3+} \rightarrow$ N$^+$ + NO^{2+} channel can be explained by the dissociation via the 1 $^2\Pi$, 2 $^2\Pi$, and 2 $^2\Sigma^-$ states of N$_2$O^{3+} along the N-N stretch direction. The theoretically predicted KER values are approximately 13.24 eV for dissociation via the 1 $^2\Pi$ state, 16.03 eV for the 2 $^2\Pi$ state, and 16.47 eV for the 2 $^2\Sigma^-$ state, in perfect agreement with the present measurement. In Fig. 3(b),

TABLE IV. The calculated energies of N$_2$O^{3+} electronic states and the KER values for N$_2$O^{3+} dissociation into N$^+$ + NO^{2+} and O$^+$ + N$_2$$^{2+}$ with various dissociation limits.

| States | Energy (eV) | N$^+$ + NO^{2+} | | O$^+$ + N$_2$$^{2+}$ | | N^{2+} + NO$^+$ | |
		Dissociation Limits	KER (eV)	Dissociation limits	KER (eV)	Dissociation limits	KER (eV)
1 $^2\Pi$	13.24	$^3P + 1$ $^2\Sigma$	13.24	$^4S^o + 1$ $^3\Pi_u$	12.66		
1 $^2\Sigma^-$	14.45	$^3P + 1$ $^2\Sigma$	15.56	$^4S^o + 1$ $^3\Sigma^-_g$	13.21		
1 $^2\Delta$	15.07	$^3P + 1$ $^2\Pi$	14.15	$^2D^o + 1$ $^1\Sigma^+_g$	11.20		
1 $^2\Sigma^+$	15.93	$^3P + 1$ $^2\Pi$	14.94	$^4S^o + 1$ $^3\Sigma^+_u$	13.83		
2 $^2\Pi$	17.58	$^3P + 1$ $^2\Pi$	16.03	$^2D^o + 1$ $^1\Sigma^+_g$	13.70		
2 $^2\Sigma^-$	18.02	$^3P + 1$ $^2\Pi$	16.47	$^2D^o + 1$ $^1\Sigma^+_g$	14.14		
3 $^2\Pi$	18.78			$^4S^o + 1$ $^3\Pi_g$	14.81	$^2P^o + 1$ $^1\Sigma$	16.65
4 $^2\Pi$	19.32	$^1D + 1$ $^2\Sigma$	17.42	$^2D^o + 1$ $^3\Pi_u$	15.42		
5 $^2\Pi$	19.57	$^1D + 1$ $^2\Pi$	16.12	$^2D^o + 1$ $^3\Pi_u$	15.67		
2 $^2\Delta$	19.87	$^1D + 1$ $^1\Sigma$	17.97	$^2D^o + 1$ $^3\Pi_u$	15.97		
3 $^2\Sigma^-$	19.88	$^1D + 1$ $^2\Pi$	16.44	$^2D^o + 1$ $^3\Pi_u$	15.99		
2 $^2\Sigma^+$	20.21			$^2D^o + 1$ $^3\Pi_u$	16.32	$^2P^o + 1$ $^1\Sigma$	18.08

for the $N_2O^{3+} \rightarrow O^+ + N_2^{2+}$ channel, the major peak at 15.0 eV can be explained by the decay of N_2O^{3+} ($3\,^2\Pi$, $4\,^2\Pi$) into $O^+(^4S^o) + N_2^{2+}(1\,^3\Pi_g)$ and $O^+(^2D^o) + N_2^{2+}(1\,^3\Pi_u)$, releasing the energies of about 14.81 and 15.42 eV. The shoulder around 12.0 eV should be mainly contributed from the dissociation via the $1\,^2\Pi$ state, whose theoretically expected KER value is about 12.66 eV, in good agreement with the experimental value. As for the $N_2O^{3+} \rightarrow N^{2+} + NO^+$ dissociation, the peak at 17.0 eV observed in Fig. 3(c) should be ascribed to the decay of the $3\,^2\Pi$ state N_2O^{3+} into $N^{2+}(^2P_0) + NO^+(1\,^1\Sigma)$ with respect to the calculated KER value of 16.65 eV. However, the explanations about the peak at 13.0 eV for $N_2O^{3+} \rightarrow N^{2+} + NO^+$ observed in Fig. 3(c) and two structures in Fig. 3(d) for $N_2O^{3+} \rightarrow O^{2+} + N_2^+$ are beyond the present theoretical calculations. The electronic states of N_2O^{3+} with other multiplicity could be responsible for them. Comprehensive calculations for the potential energy curves of N_2O^{3+} are expected to further investigate the specific pathways of $N_2O^{3+} \rightarrow N^{2+} + NO^+$ and $O^{2+} + N_2^+$ in the future.

V. CONCLUSION

Two-body fragmentation of N_2O^{q+} ($q = 2, 3$) induced by the EC reactions of 5.7-keV/u Xe^{15+} collision are investigated by utilizing a reaction microscope. Twelve reaction channels have been identified from the two-dimensional TOF correlation maps of ion-pair fragments measured in coincidence with the charge-changed projectile. The relative fractions of these 12 reaction channels are also determined and the corresponding KER distributions for the specific dissociations of N_2O^{2+} and N_2O^{3+} have been derived. The potential energy curves of N_2O^{3+} are calculated at the CASSCF level of theory. We found that the N_2O^{2+} prefers to dissociate along the N-N direction via the $1\,^3\Sigma^-$ state to the $N^+(^3P) + NO^+(^1\Sigma^+)$ pathway and decay along the N-O bond via the $X\,^3\Sigma^-$ and $1\,^3\Pi$ states into $O^+(^4S) + N_2^+(^2\Sigma_g^+)$ and $O^+(^4S) + N_2^+(^2\Pi_u)$, respectively. For the fragmentation of N_2O^{3+}, the dominant pathways are proposed that the low-lying states ($1\,^2\Pi$, $2\,^2\Pi$, and $2\,^2\Sigma^-$) mainly result in $N^+(^3P) + NO^{2+}(1\,^2\Sigma)$ and $N^+(^3P) + NO^{2+}(1\,^2\Pi)$, whereas higher excited states ($3\,^2\Pi$ and $4\,^2\Pi$) prefer to dissociate into $O^+(^4S^o) + N_2^{2+}(1\,^3\Pi_g)$ and $O^+(^2D^o) + N_2^{2+}(1\,^3\Pi_u)$. In addition, we also found that the behavior characteristics of KER distributions, particularly at the peaks or structures and their positions, for the same ion-pair fragments of N_2O^{2+} and N_2O^{3+} are not sensitive to the number of electrons stabilized on the projectile in the reaction processes, which are different from the previous observations of Ehrich *et al.* [7] in slow collisions of 300-keV Ar^{3+} with N_2 and those of Watson *et al.* [27] in fast collisions of 97-MeV Ar^{14+} with CO. In present slow collisions of highly charged Xe^{15+} with N_2O, the electron-capture process of projectile ions should be most dominant and the possibility of direct ionization of targets is quite small, which is similar to the observation in the low-velocity ion collision with atoms or molecules [18,47]. We conjecture that the present reaction is the capture of k electrons into multiply excited levels of projectile with the formation of a transient k-fold multicharged molecule, i.e., $Xe^{15+} + N_2O \rightarrow [Xe^{(15-k)+}]^{**} + [N_2O^{k+}]^{**}$ ($k = 2, 3$), which is followed by a projectile stabilization with or without autoionizing cascades ($[Xe^{(15-k)+}]^{**} \rightarrow Xe^{(15-k+m)+} + me^-$, $m = 0, 1, 2$) and accompanied by kinds of fragmentation from molecular ions. Such electron-capture processes in the collision could induce almost identical state populations of N_2O^{k+}, which is a possible reason that the present KER distributions show almost the same feature for the specific ion-pair fragments of N_2O^{2+} and N_2O^{3+} measured in coincidence with Xe^{13+} and Xe^{14+} scattered projectiles. Further experiments on the N_2O molecule are desirable to investigate this issue by using additional electron coincidence measurement or using other kinds of ion projectiles with different charges and energies in the future.

[1] N. Neumann, D. Hant, L. P. H. Schmidt, J. Titze, T. Jahnke, A. Czasch, M. S. Schöffler, K. Kreidi, O. Jagutzki, H. Schmidt-Böcking, and R. Dörner, Phys. Rev. Lett. **104**, 103201 (2010).

[2] H.-K. Kim, J. Titze, M. Schoffler, F. Trinter, M. Waitz, J. Voigtsberger, H. Sann, M. Meckel, C. Stuck, U. Lenz, M. Odenweller, N. Neumann, S. Schossler, K. Ullmann-Pfleger, B. Ulrich, R. C. Fraga, N. Petridis, D. Metz, A. Jung, R. Grisenti *et al.*, Proc. Natl. Acad. Sci. USA **108**, 11821 (2011).

[3] R. Dörner, V. Mergel, O. Jagutzki, L. Spielberger, J. Ullrich, R. Moshammer, and H. Schmidt-Böcking, Phys. Rep. **330**, 95 (2000).

[4] J. Ullrich, R. Moshammer, A. Dorn, R. Dörner, L. P. H. Schmidt, and H. Schmidt-Böcking, Rep. Prog. Phys. **66**, 1463 (2003).

[5] J. Rajput, S. De, A. Roy, and C. P. Safvan, Phys. Rev. A **74**, 032701 (2006).

[6] A. Méry, A. N. Agnihotri, J. Douady, X. Fléchard, B. Gervais, S. Guillous, W. Iskandar, E. Jacquet, J. Matsumoto, J. Rangama, F. Ropars, C. P. Safvan, H. Shiromaru, D. Zanuttini, and A. Cassimi, Phys. Rev. Lett. **118**, 233402 (2017).

[7] M. Ehrich, B. Siegmann, U. Werner, and H. Lebius, Radiat. Phys. Chem. **68**, 127 (2003).

[8] T. Kaneyasu, T. Azuma, and K. Okuno, J. Phys. B: At. Mol. Opt. Phys. **38**, 1341 (2005).

[9] B. Siegmann, U. Werner, R. Mann, N. M. Kabachnik, and H. O. Lutz, Phys. Rev. A **62**, 022718 (2000).

[10] T. Mizuno, T. Yamada, H. Tsuchida, Y. Nakai, and A. Itoh, Phys. Rev. A **82**, 054702 (2010).

[11] H. O. Folkerts, R. Hoekstra, and R. Morgenstern, Phys. Rev. Lett. **77**, 3339 (1996).

[12] E. Wells, V. Krishnamurthi, K. D. Carnes, N. G. Johnson, H. D. Baxter, D. Moore, K. M. Bloom, B. M. Barnes, H. Tawara, and I. Ben-Itzhak, Phys. Rev. A **72**, 022726 (2005).

[13] H. O. Folkerts, T. Schlathölter, R. Hoekstra, and R. Morgenstern, J. Phys. B: At. Mol. Opt. Phys. **30**, 5849 (1997).

[14] J. Rajput and C. P. Safvan, Phys. Rev. A **75**, 062709 (2007).

[15] A. Khan, L. C. Tribedi, and D. Misra, Phys. Rev. A **92**, 030701 (2015).

[16] D. Mathur, E. Krishnakumar, F. A. Rajgara, U. T. Raheja, and V. Krishnamurthi, J. Phys. B: At. Mol. Opt. Phys. **25**, 2997 (1992).

[17] S. Yan, X. L. Zhu, P. Zhang, X. Ma, W. T. Feng, Y. Gao, S. Xu, Q. S. Zhao, S. F. Zhang, D. L. Guo, D. M. Zhao, R. T. Zhang, Z. K. Huang, H. B. Wang, and X. J. Zhang, Phys. Rev. A **94**, 032708 (2016).

[18] P. Moretto-Capelle, D. Bordenave-Montesquieu, and A. Bordenave-Montesquieu, J. Phys. B: At. Mol. Opt. Phys. **33**, L735 (2000).

[19] B. Wales, T. Motojima, J. Matsumoto, Z. Long, W.-K. Liu, H. Shiromaru, and J. Sanderson, J. Phys. B: At. Mol. Opt. Phys. **45**, 45205 (2012).

[20] M. R. Jana, P. N. Ghosh, B. Ray, B. Bapat, R. K. Kushawaha, K. Saha, I. A. Prajapati, and C. P. Safvan, Eur. Phys. J. D **68**, 250 (2014).

[21] F. A. Rajgara, M. Krishnamurthy, D. Mathur, T. Nishide, T. Kitamura, H. Shiromaru, Y. Achiba, and N. Kobayashi, Phys. Rev. A **64**, 032712 (2001).

[22] W. Wolff, H. Luna, R. Schuch, N. D. Cariatore, S. Otranto, F. Turco, D. Fregenal, G. Bernardi, and S. Suárez, Phys. Rev. A **94**, 022712 (2016).

[23] B. Siegmann, U. Werner, H. O. Lutz, and R. Mann, J. Phys. B: At. Mol. Opt. Phys. **34**, L587 (2001).

[24] K. Béroff, N. T. Van-Oanh, M. Chabot, T. Tuna, T. Pino, G. Martinet, A. Le Padellec, Y. Carpentier, and L. Lavergne, Phys. Rev. A **84**, 032705 (2011).

[25] S. Xu, X. L. Zhu, W. T. Feng, D. L. Guo, Q. Zhao, S. Yan, P. Zhang, D. M. Zhao, Y. Gao, S. F. Zhang, J. Yang, and X. Ma, Phys. Rev. A **97**, 062701 (2018).

[26] Y. Zhang, T. Jiang, L. Wei, D. Luo, X. Wang, W. Yu, R. Hutton, Y. Zou, and B. Wei, Phys. Rev. A **97**, 022703 (2018).

[27] R. L. Watson, G. Sampoll, V. Horvat, and O. Heber, Phys. Rev. A **53**, 1187 (1996).

[28] A. R. Ravishankara, J. S. Daniel, and R. W. Portmann, Science **326**, 123 (2009).

[29] A. Khan and D. Misra, J. Phys. B: At. Mol. Opt. Phys. **49**, 055201 (2016).

[30] P. Bhatt, R. Singh, N. Yadav, and R. Shanker, Phys. Rev. A **86**, 052708 (2012).

[31] N. A. Love and S. D. Price, Phys. Chem. Chem. Phys. **6**, 4558 (2004).

[32] J. H. D. Eland and V. J. Murphy, Rapid Commun. Mass Spectrom. **5**, 221 (1991).

[33] M. Alagia, P. Candori, S. Falcinelli, M. Lavollée, F. Pirani, R. Richter, S. Strangesand, and F. Vecchiocattivi, Chem. Phys. Lett. **432**, 398 (2006).

[34] S. D. Price, J. H. D. Eland, P. G. Fournier, J. Fournier, and P. Millie, J. Chem. Phys. **88**, 1511 (1988).

[35] S. Taylor, J. H. D. Eland, and M. Hochlaf, J. Chem. Phys. **124**, 204319 (2006).

[36] D. M. Curtis and J. H. D. Eland, Int. J. Mass Spectrom. Ion Processes **63**, 241 (1985).

[37] X. Zhou, P. Ranitovic, C. W. Hogle, J. H. D. Eland, H. C. Kapteyn, and M. M. Murnane, Nat. Phys. **8**, 232 (2012).

[38] M. Kübel, A. S. Alnaser, B. Bergues, T. Pischke, J. Schmidt, Y. Deng, C. Jendrzejewski, J. Ullrich, G. G. Paulus, A. M. Azzeer, U. Kleineberg, R. Moshammer, and M. F. Kling, New J. Phys. **16**, 065017 (2014).

[39] A. Hishikawa, A. Iwamae, K. Hoshina, M. Kono, and K. Yamanouchi, Res. Chem. Intermed. **24**, 765 (1998).

[40] M. Ueyama, H. Hasegawa, A. Hishikawa, and K. Yamanouchi, J. Chem. Phys. **123**, 154305 (2005).

[41] N. Levasseur and P. Millié, J. Chem. Phys. **92**, 2974 (1990).

[42] B. Siegmann, U. Werner, H. O. Lutz, and R. Manny, *GSI Scientific Report 2002* (2003), p. 100, https://repository.gsi.de/record/53529.

[43] D. Wang, G. Guo, G. Min, and X. Zhang, Phys. Rev. A **95**, 012705 (2017).

[44] U. Werner, B. Siegmann, and R. Mann, *GSI Scientific Report 2006* (2007), p. 253, https://repository.gsi.de/record/53525.

[45] A. Khan, L. C. Tribedi, and D. Misra, Phys. Rev. A **96**, 012703 (2017).

[46] X. Ma, X. Zhu, H. Liu, B. Li, S. Zhang, S. Cao, W. Feng, and S. Xu, Sci. China Ser. G: Phys. Mech. Astron. **51**, 755 (2008).

[47] X. Ma, R. T. Zhang, S. F. Zhang, X. L. Zhu, W. T. Feng, D. L. Guo, B. Li, H. P. Liu, C. Y. Li, J. G. Wang, S. C. Yan, P. J. Zhang, and Q. Wang, Phys. Rev. A **83**, 052707 (2011).

[48] W. C. Wiley and I. H. McLaren, Rev. Sci. Instrum. **26**, 1150 (1955).

[49] P. J. Knowles and H.-J. Werner, Chem. Phys. Lett. **115**, 259 (1985).

[50] H. J. Werner and P. J. Knowles, J. Chem. Phys. **82**, 5053 (1985).

[51] T. H. Dunning, Jr., J. Chem. Phys. **90**, 1007 (1989).

[52] H.-J. Werner, P. J. Knowles, G. Knizia, F. R. Manby, M. Schütz, P. Celani, T. Korona, R. Lindh, A. Mitrushenkov, G. Rauhut, K. R. Shamasundar, T. B. Adler, R. D. Amos, A. Bernhardsson, A. Berning, D. L. Cooper, M. J. O. Deegan, A. J. Dobbyn, F. Eckert, E. Goll *et al.*, MOLPRO, a package of *ab initio* programs, version 2010.1 (2010). See http://www.molpro.net.

[53] R. Murphy and W. Eberhardt, J. Chem. Phys. **89**, 4054 (1988).

[54] E. Wang, M. Gong, Z. Shen, X. Shan, X. Ren, A. Dorn, and X. Chen, J. Chem. Phys. **149**, 204301 (2018).